This is a repository copy of *Anion-Mediated Photophysical Behavior in a C60 Fullerene [3]Rotaxane Shuttle*.

White Rose Research Online URL for this paper:
http://eprints.whiterose.ac.uk/130287/

Version: Accepted Version

Article:

Anion mediated photophysical behavior in a C_{60} fullerene [3]rotaxane shuttle

Timothy A. Barendt,[†] Ilija Rašović,[‡] Maria A. Lebedeva,[‡] George A. Farrow,[⊥] Alexander Auty,[⊥] Dimitri Chekulaev,[⊥] Igor V. Sazanovich,[&] Julia A. Weinstein,[⊥] Kyriakos Porfyrakis[‡] and Paul D. Beer*[†]

[†]Chemistry Research Laboratory, Department of Chemistry, University of Oxford, Mansfield Road, Oxford OX1 3TA, United Kingdom

[‡]Department of Materials, University of Oxford, Parks Road, Oxford OX1 3PH, United Kingdom

[⊥]Department of Chemistry, University of Sheffield, Sheffield S3 7HF, United Kingdom

[&]Laser for Science Facility, Rutherford Appleton Laboratory, Research Complex at Harwell, OX11 0QX, United Kingdom

ABSTRACT: By addressing the challenge of controlling molecular motion, mechanically interlocked molecular machines are primed for a variety of applications in the field of nanotechnology. Specifically, the designed manipulation of communication pathways between electron donor and acceptor moieties that are strategically integrated into dynamic photoactive rotaxanes and catenanes may lead to efficient artificial photosynthetic devices. In this pursuit, a novel [3]rotaxane molecular shuttle consisting of a four station bis-naphthalene diimide (NDI) and central C_{60} fullerene bis-triazolium axle component and two mechanically bonded ferrocenyl functionalized -isophthalamide anion binding site-containing macrocycles is constructed using an anion template synthetic methodology. Dynamic co-conformational anion recognition mediated shuttling which alters the relative positions of the electron donor and acceptor motifs of the [3]rotaxane's macrocycle and axle components is demonstrated initially by ^{1}H NMR spectroscopy. Detailed steady state and time-resolved UV–Vis–IR absorption and emission spectroscopies as well as electrochemical studies are employed to further probe the anion dependent positional macrocycle–axle station state of the molecular shuttle, revealing a striking on/off switchable emission response induced by anion binding. Specifically, the [3]rotaxane chloride co-conformation, where the ferrocenyl functionalized macrocycles reside at the center of the axle component, precludes electron transfer to NDI, resulting in the switching-on of emission from the NDI fluorophore and concomitant formation of a C_{60} fullerene-based charge separated state. By stark contrast, in the absence of chloride as the hexafluorophosphate salt, the ferrocenyl functionalized macrocycles shuttle to the peripheral NDI axle stations, quenching the NDI emission via formation of a NDI-containing charge separated state. Such anion mediated control of the photophysical behavior of a rotaxane through molecular motion is unprecedented.

Introduction

The potential for synthetic molecular machines to fuel the nanotechnological revolution relies upon the ability of chemists to construct systems in which the motion of individual molecules may be controlled and directed.[1–3] As a consequence, attention has turned towards mechanically interlocked molecules (MIMs) such as rotaxanes and catenanes in which their inherent dynamic properties are restricted by a mechanical bond.[4,5] Through the biasing of remaining accessible Brownian motions, the MIM may be forced into adopting a well-defined spatial arrangement of its interlocked components known as a co-conformation.[6] By careful design, systems may be constructed that can interconvert between two or more co-conformations; for example the shuttling of a macrocycle between two stations on an axle in a [2]rotaxane.[7–10] This switching process can be triggered by a variety of light,[11–13] redox[14,15] or chemical[16,17] based external stimuli. In the latter case, examples of MIM dynamic behavior controlled by discrete anion recognition are rare.[18–28] This is especially so with

1

higher-order interlocked structures containing more than two mechanically bonded components where anion mediated co-conformational switching can induce a variety of large-amplitude molecular motions including the translation and rotation of macrocyclic rings in a [3]rotaxane[29] and a [3]catenane respectively.[30] Systems of this type, which exhibit excellent positional integrity between co-conformations,[18] may be exploited for the development of photoactive switchable devices,[31] where electron donor(D)–electron acceptor(A) communication pathways between appropriately functionalized interlocked components can be controlled dynamically via anion recognition, resulting in distinct and switchable photophysical behavior.
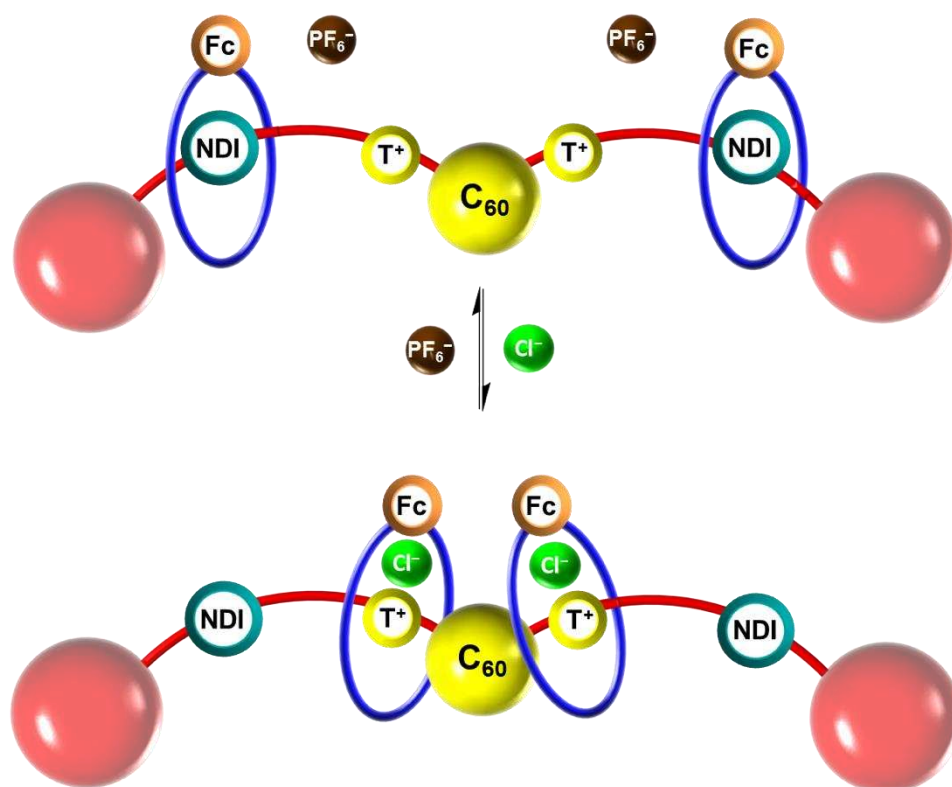

Figure 1: Schematic showing co-conformational switching in a dynamic D–A four-station C_{60} fullerene-containing [3]rotaxane via anion induced molecular motion of a macrocycle (blue) between stations (green and yellow) along an axle (red). NDI = naphthalene diimide, T^+ = triazolium and Fc = ferrocene.

C_{60} fullerene[32] is an attractive functional building block to incorporate into MIM structural frameworks due to its ~1 nm size and spherical shape as a sterically bulky stoppering unit for rotaxanes.[33,34] However, to the best of our knowledge, no higher-order interlocked structures containing fullerenes have been reported. Importantly, C_{60} fullerene also possesses unique redox properties[35–38] and is a strong electron acceptor (A)[33,39–46] which can be used to probe molecular motion in dynamic donor–acceptor-containing MIMs and exploited to control intramolecular photoinduced charge separation processes,[34,47] that mimic a key step in photosynthesis.[48] For example, the proximity of a ferrocene-containing macrocycle (D) to a C_{60} fullerene stoppered axle component (A) in a bistable [2]rotaxane was controlled by varying the nature of the bulk solvent, which provided the means to change the lifetime of the charge separated excited state.[49]

Herein, we describe the design, synthesis and comprehensive photophysical investigation of a novel multifunctional dynamic [3]rotaxane. The system is comprised of a four station axle component containing two peripheral fluorescent electron accepting naphthalene diimide (NDI) units and a centrally positioned electron deficient C_{60} fullerene bis-triazolium motif, and two mechanically bonded ferrocenyl-isophthalamide anion binding site-containing macrocycles (Figure 1). This D–A molecular shuttle is demonstrated to adopt two distinct and anion-dependent co-conformations that interconvert via large amplitude translational motion of both ferrocenyl macrocycle components (D) between the peripheral NDI (A) and central triazolium-bridged C_{60} (A) axle stations. The difference in the photophysical response arising

2

from anion recognition changing the spatial separation of the interlocked D–A motifs has been comprehensively probed and characterized by steady state and time resolved absorption, infrared and emission spectroscopies. A fullerene containing [3]rotaxane is unprecedented and represents the first multicomponent MIM system in which photophysical behavior is controlled via anion mediated molecular motion.

Synthesis of [3]rotaxane

The [3]rotaxane was synthesized by a multistep synthetic pathway as detailed in the Supporting Information (SI). This began with the preparation of the symmetric C_{60} fullerene-based four-station axle component containing two triazolium and two NDI motifs via successive Bingel,[50,51] copper-catalyzed azide-alkyne cycloaddition (CuAAC) 'click' and alkylation reactions, and isolated as the bis-chloride salt **1·(Cl)$_2$**. For mechanical bond formation, the chloride anion template clipping of two bis-vinyl-functionalized 5-ferrocenyl-isophthalamide macrocycle precursors[52] around the axle component by Grubbs' II catalyzed ring closing metathesis in dry dichloromethane was employed (Scheme 1). Following purification by preparative silica thin-layer chromatography the target [3]rotaxane **3·(Cl)$_2$** was obtained in an isolated yield of 11% together with the analogous [2]rotaxane **4·(Cl)$_2$** (15%) and macrocyclic and unreacted axle side products. The [3]rotaxane **3·(Cl)$_2$** was anion exchanged to the bis-hexafluorophosphate salt using Amberlite® resin to give **3·(PF$_6$)$_2$**. Both [3]rotaxane salts were fully characterized by ^{1}H, ^{13}C and two-dimensional ^{1}H ROESY NMR spectroscopy and matrix-assisted laser desorption/ionization (MALDI) mass spectrometry (see SI).

3
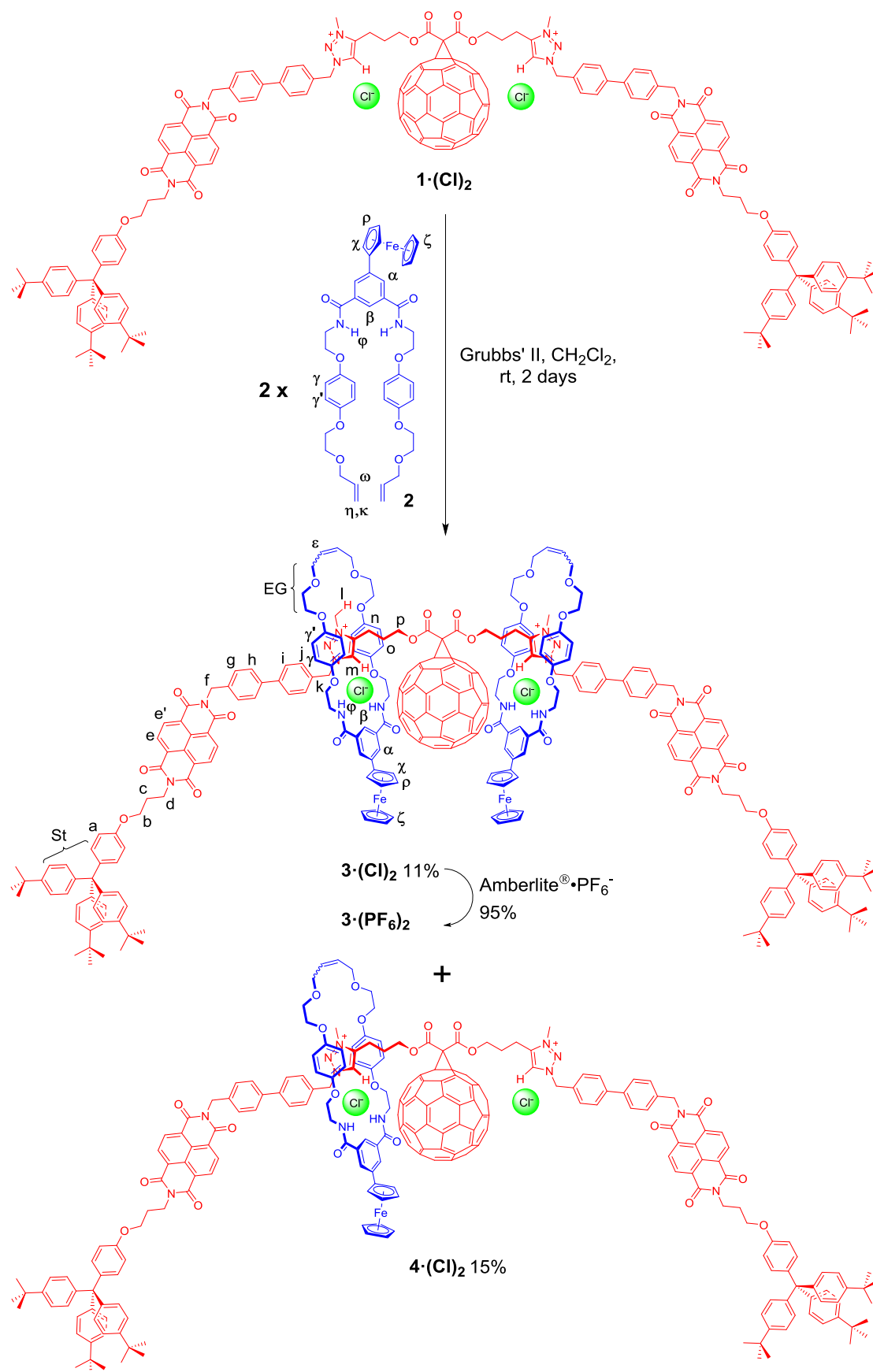
Scheme 1. Chloride templated syntheses of the [3] and [2]rotaxanes.

4

^{1}H NMR spectroscopy molecular motion investigations

Initially the dynamic properties of the four-station [3]rotaxane were investigated by determining the co-conformations of the molecular shuttle as the coordinating (bis-chloride) $3 \cdot (Cl)_2$ and non-coordinating (bis-hexafluorophosphate) $3 \cdot (PF_6)_2$ anion salts in CDCl$_3$ solution using one- and two-dimensional ^{1}H NMR spectroscopy.

A comparison of the ^{1}H NMR spectrum of $3 \cdot (Cl)_2$ with spectra of the C$_{60}$ fullerene-containing axle component $1 \cdot (Cl)_2$ and ferrocenyl-based macrocycle precursor 2 revealed a downfield shift of macrocycle isophthalamide proton H$_\beta$, whilst the axle triazolium signal H$_m$ moved upfield (Figure 2). This is indicative of hydrogen bonding anion recognition of chloride in each of the interlocked cavities created between the macrocycle isophthalamide cleft and the axle triazolium station of the orthogonally arranged macrocycle and axle components. Peaks associated with the macrocycle hydroquinone environments H$_{\gamma,\gamma'}$ were also significantly shifted upfield ($\Delta\delta$ = 0.40 ppm) in $3 \cdot (Cl)_2$, due to ring current effects from the neighboring C$_{60}$ fullerene cage.[53–55] Finally, either side of the biphenyl spacer in the multi-station axle, only the H$_k$ methylene signal was found to be perturbed upon formation of the [3]rotaxane. This provided further evidence that under these conditions the macrocycles reside at the axle triazolium anion recognition sites. As such, strong through-space couplings between protons associated with the triazolium station (H$_{i,j,k,l}$) and the proximal macrocyclic ring (H$_{\gamma,\gamma',\beta,\varepsilon}$) were observed in the two-dimensional ^{1}H ROESY NMR spectrum of $3 \cdot (Cl)_2$ (Figure S2).

Interestingly the ^{1}H NMR spectrum of the analogous [2]rotaxane $4 \cdot (Cl)_2$ was more complex owing to the fact the central C$_{60}$ fullerene motif sterically restricts macrocycle translocation to each half of the axle (Figure S1). Therefore, desymmetrization of the axle component in the [2]rotaxane splits proton signals into two distinct sets arising from the presence or absence of a macrocycle. However, this is only true for proton environments associated with the triazolium station (e.g. H$_{k,m}$), not NDI (e.g. H$_{e,f}$), and so further supports a co-conformation of [3]rotaxane $3 \cdot (Cl)_2$ in which both macrocycles occupy the axle triazolium stations either side of the fullerene.

Comparison of the ^{1}H NMR spectra of the bis-chloride and bis-hexafluorophosphate salts of the [3]rotaxane indicated translational motion of both macrocycle components occurs upon anion exchange from chloride to hexafluorophosphate, triggering the macrocyclic rings to move from the axle triazolium stations to reside at the peripheral NDI stations (Figure 3). Specifically, anion exchange produced large upfield shifts of macrocycle hydroquinone H$_{\gamma,\gamma'}$ ($\Delta\delta$ = 0.18 ppm) and axle NDI H$_{e,e'}$ resonances ($\Delta\delta$ = 0.18 ppm) due to the formation of strong aromatic stacking interactions between the components whilst perturbation of the nearby methylene peak (H$_f$) provided further support for this co-conformational change. The removal of chloride produced diagnostic upfield shifts of acidic protons H$_m$ and H$_{\beta,\varphi}$ at the anion binding station, albeit for the latter not back to their original position in macrocycle precursor 2, indicating the possibility of supplementary hydrogen bonding between the isophthalamide motif of the macrocycle and carbonyl groups of the NDI stations (Figure 3).[20,56] Finally, the appearance of new peaks in the two-dimensional ^{1}H ROESY NMR spectrum of $3 \cdot (PF_6)_2$ indicated the proximity of protons on the macrocyclic wheels (H$_{\varepsilon,\gamma,\gamma'}$) to those associated with the NDI stations (H$_{a',e,e'}$) (Figure S3).

In order to quantitatively assess the anion-induced co-conformational change exhibited by the [3]rotaxane, the percentage of macrocycles occupying the triazolium or NDI stations was calculated for both bis-hexafluorophosphate and bis-chloride salts in CDCl$_3$ (Figure 4). Since the dynamic behavior of the [3]rotaxanes was fast on the ^{1}H NMR timescale this was achieved by comparing the chemical shift of NDI station protons H$_{e,e'}$ of [3]rotaxanes $3 \cdot (A)_2$ with that of the same signals in axle component $1 \cdot (A)_2$ and a model NDI-only-containing [2]rotaxane which characterize the two extremes of macrocycle–station occupancy, 0% and 100% respectively (see SI Section 3).[18] These studies revealed an excellent positional integrity between macrocycle sites in each of the anion states with anion exchange between bis-chloride and bis-hexafluorophosphate salts stimulating 80% of the rings to shuttle between triazolium and NDI stations (Figure 4). In summary, [3]rotaxane $3 \cdot (A)_2$ exhibits anion controlled, reversible and large-amplitude translational motion of both ferrocenyl macrocycle components along the C$_{60}$ and NDI-containing four-station axle component in CHCl$_3$ solution. With NMR characterization of the dynamic properties of this higher order interlocked structure in hand, attention turned towards investigating the effect of these co-conformational changes on the photophysical properties of the system.
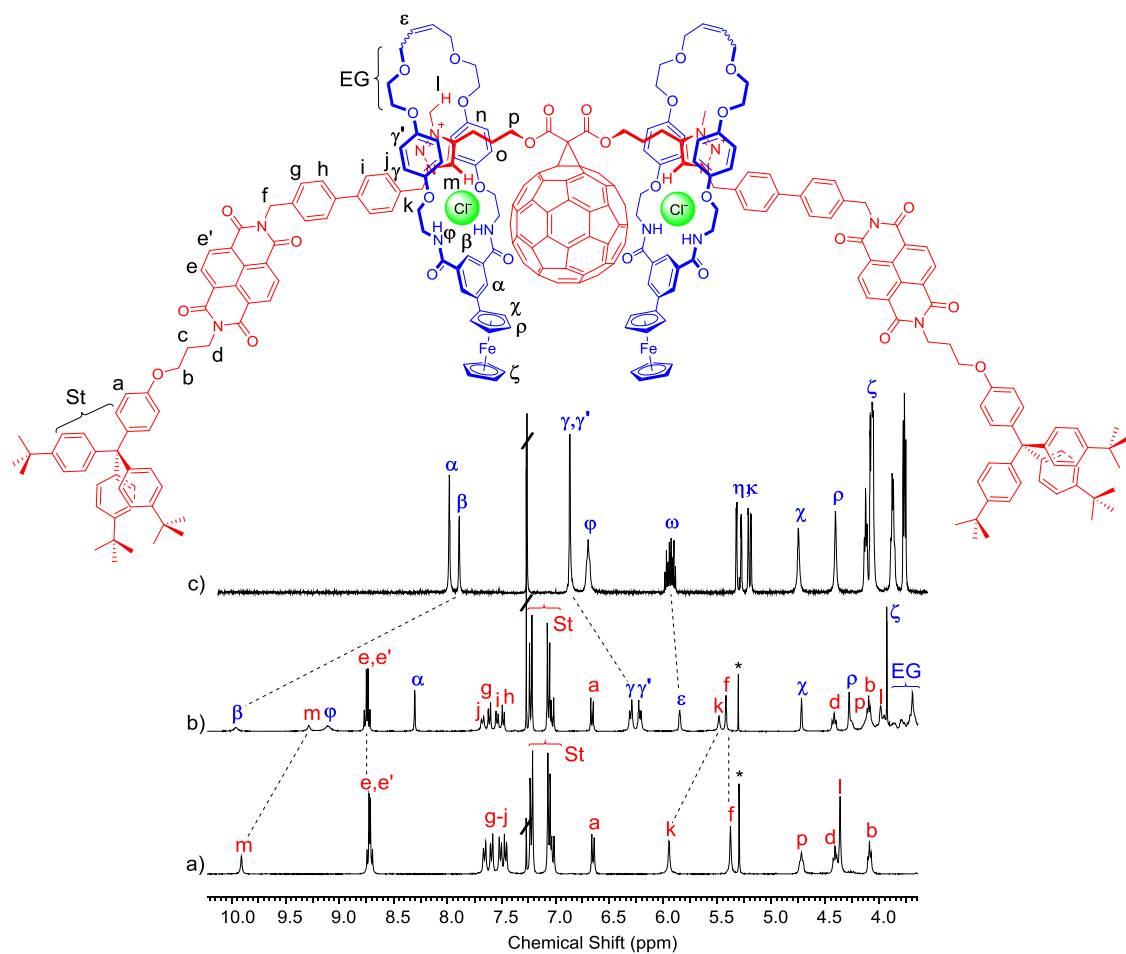
Figure 2. Comparison of ^{1}H NMR spectra of a) axle component **1·(Cl)$_2$**, b) [3]rotaxane **3·(Cl)$_2$** and c) ferrocenyl-isophthalamide macrocycle precursor **2** provides evidence for the dominant co-conformation of [3]rotaxane **3·(Cl)$_2$** as depicted above (CDCl$_3$, 298 K, 400 MHz). Additional proton signals: St = axle stopper, EG = macrocycle ethylene glycol and * = trace residual solvent.

Figure 3. Comparison of ¹H NMR spectra of the [3]rotaxane **3·(A)₂** as the a) bis-hexafluorophosphate and b) bis-chloride salt reveals co-conformational change via translational motion of ferrocenyl macrocycle components (CDCl₃, 298 K, 400 MHz). Additional proton signals: St = axle stopper, EG = macrocycle ethylene glycol and * = trace residual solvent.

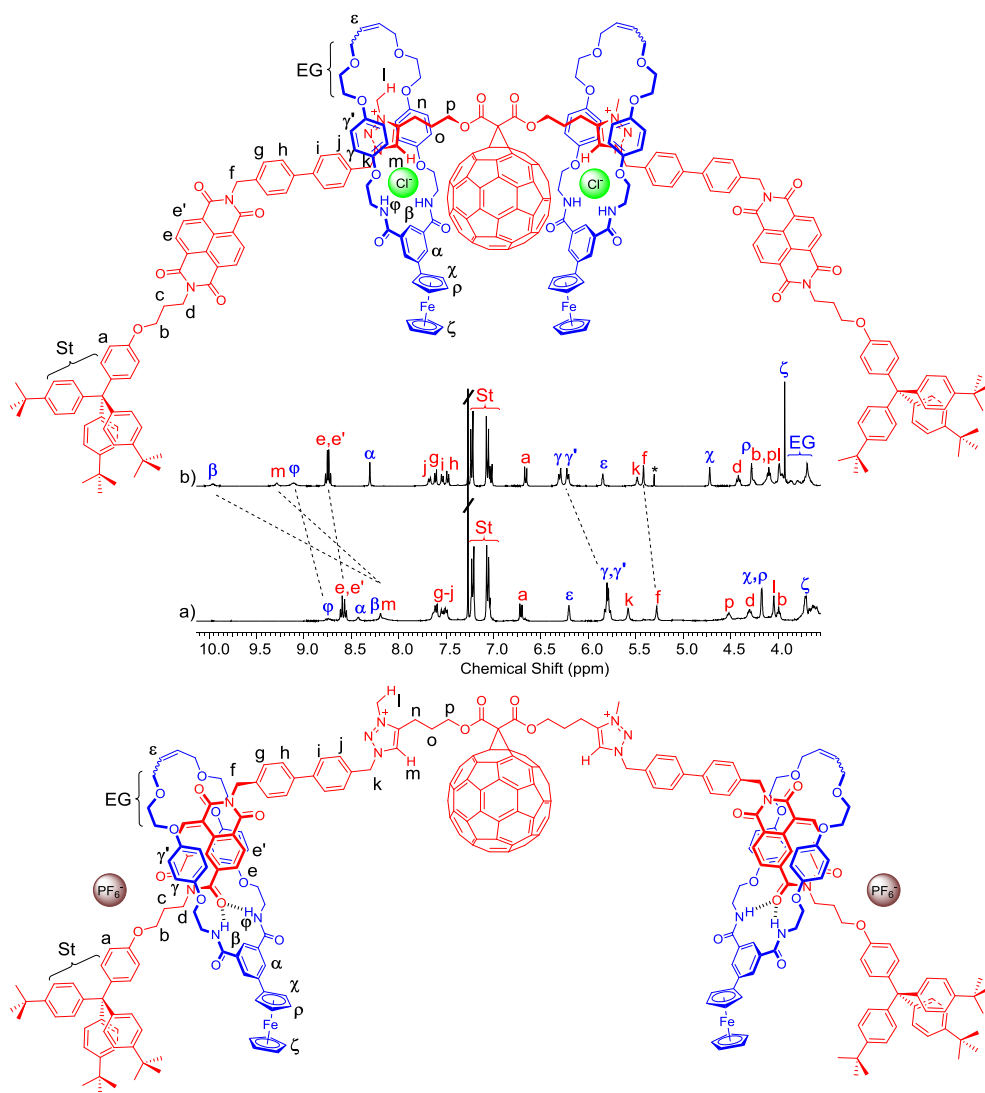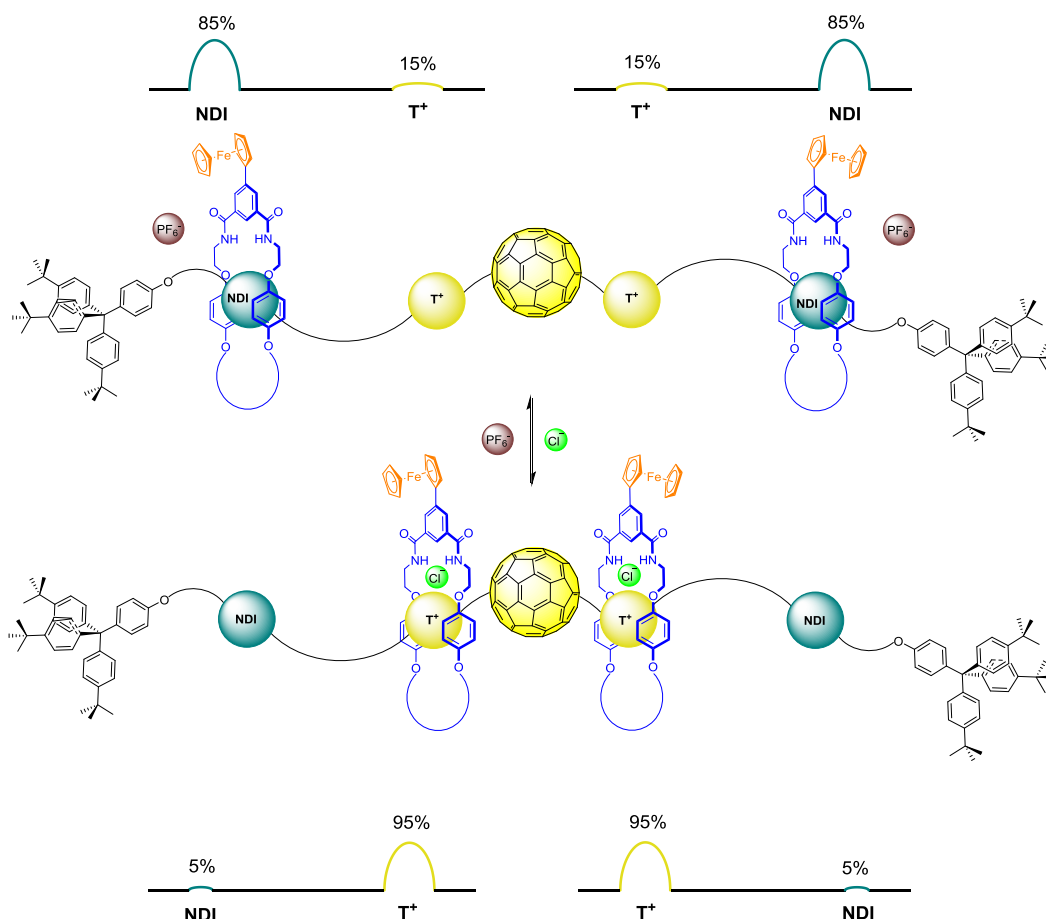Figure 4. Estimated macrocycle–station occupancies of [3]rotaxane **3·(A)₂** as the bis-hexafluorphosphate and bis-chloride salt as determined by ¹H NMR spectroscopy in CDCl₃ solution. T⁺ = triazolium.

Steady state absorption and infrared spectroscopy

Steady state absorption spectra of [3]rotaxane salts **3·(Cl)₂** and **3·(PF₆)₂** were recorded in CHCl₃ (10 μM) (Figure S8). Both exhibited strong, structured absorptions in the UV region (360 nm: **3·(Cl)₂**, ε = 20,310 M^{-1} cm^{-1}; **3·(PF₆)₂**, ε = 17,200 M^{-1} cm^{-1}), characteristic of an NDI derivative[57] whilst the typical absorption signature of C_{60} methanofullerene, namely a small shoulder at 425 nm,[58,59] was also evident. Similar absorptions for NDI and C_{60} motifs were also present in the UV-Vis spectra of the analogous salts of the axle component, **1·(Cl)₂** and **1·(PF₆)₂** (Figure S9). The ratio of peaks in the vibronic fine structure of the NDI absorption band differed very slightly on comparison of each axle to its corresponding [3]rotaxane salt, suggestive of only a small degree of electronic communication between the mechanically interlocked components in the [3]rotaxane. As a consequence, only a small difference was observed on comparison of the absorption spectra of [3]rotaxanes **3·(Cl)₂** and **3·(PF₆)₂**, namely a slight broadening of each NDI feature in the spectrum of the latter, indicative of intramolecular charge transfer involving the NDI unit[60] caused by aromatic stacking interactions with the macrocycle hydroquinone groups.[18] However, in general these observations indicate that changing the nature of the counter anion has only a minor influence on the electronic ground state of the [3]rotaxane despite significantly altering the co-conformation. These conclusions were supported by electrochemical studies (*vide infra*).

The steady state infrared (IR) spectra recorded in dichloromethane[61] revealed multiple IR bands in the fingerprint region, including those of *v*(CO) of the NDI (1706 and 1666 cm^{-1}), C_{60}-linked malonate group (a broad band at 1740 cm^{-1}), *v*(CO) of the macrocyclic amide group of the rotaxane, at approx. 1645 cm^{-1}, a band at 1585 cm^{-1} (the naphthalene core of the NDI) and bands at 1550 and 1505 cm^{-1} which are assigned to the axle biphenyl moieties (Figure S10). Interestingly, the ratio of the NDI carbonyl absorption bands differed between the [3]rotaxane anion salts, consistent with the ¹H NMR spectroscopic evidence of hydrogen

bonding interactions between these groups and the isophthalamide clefts of the macrocycle components when the rings occupy the axle NDI stations in **3·(PF$_6$)$_2$** (Figure 3).[20,56]

Electrochemical characterization

Cyclic voltammograms of both [3]rotaxane salts, as well as all of the individual building blocks, were recorded in dimethylformamide containing 0.2 M [^{n}Bu$_4$N][BF$_4$] or LiCl as supporting electrolytes for compounds containing non-coordinating or coordinating anion salts respectively (Table 1 and SI Section 5).[62,63]

Table 1. Electrochemical data of the rotaxane samples **3·(Cl)$_2$** and **3·(PF$_6$)$_2$** and the corresponding building blocks recorded in DMF/LiCl or DMF/[^{n}Bu$_4$N][BF$_4$] respectively. All electrochemical potentials quoted *vs.* Fc$^+$/Fc redox couple.

Salt	Compound	$E_{1/2}$ **Ox** [a] (Fc), V	$E_{1/2}$**red$_1$** (C$_{60}$), V	$E_{1/2}$**red$_1$** (NDI), V	$E_{1/2}$**red$_2$** (C$_{60}$), V	$E_{1/2}$**red$_2$** (NDI), V	$E_{1/2}$**red$_3$** (C$_{60}$), V	$E_{1/2}$**red$_1$** (Trz.), V
	NDI	-	-	-0.94	-	-1.35	-	-
	C$_{60}$ malonate	-	-0.80	-	-1.27	-	-	-
	Triazolium	-	-	-	-	-	-	-2.09
Cl	Axle **1·(Cl)$_2$**	-	-0.80	-0.94	-1.26	-1.32	-	-
	Fc macrocycle precursor **2**	+0.02	-	-	-	-	-	-
	[3]Rotaxane, **3·(Cl)$_2$**	+0.03	-0.82	-0.96	-1.27[64]	-1.32		-
	NDI	-	-	-0.93	-	-1.43	-	-
	C$_{60}$ malonate	-	-0.80	-	-1.26	-	-1.84	-
	Axle, **1·(PF$_6$)$_2$**	-	-0.80	-0.95	-1.23	-1.42	-1.79	-
PF$_6$	Fc macrocycle precursor **2**	+0.06	-	-	-	-	-	-
	[3]Rotaxane, **3·(PF$_6$)$_2$**	+0.07	-0.81	-0.96	-1.25	-1.41	-1.82	-

[a] Potentials ($E_{1/2}$ = (E_p^a + E_p^c)/2) in V quoted to the nearest 0.01 V. All potentials are reported against the Fc$^+$/Fc couple for 0.5 – 1.0 mM solutions in DMF containing 0.2 M of the corresponding supporting electrolyte. The structures of compounds containing only NDI, triazolium (Trz.) or C$_{60}$ malonate derivatives are shown in the SI Section 5.
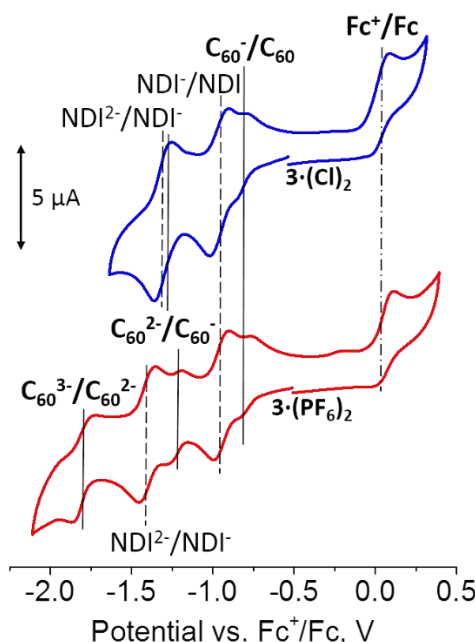
Figure 5. Cyclic voltammograms of **3·(Cl)$_2$** (top) and **3·(PF$_6$)$_2$** (bottom) recorded in DMF containing either 0.2 M LiCl or [^{n}Bu$_4$N][BF$_4$] respectively as supporting electrolyte at 0.1 V/s. Solid lines indicate the E$_{1/2}$ of the fullerene-based redox processes, dashed lines indicate the E$_{1/2}$ position of the NDI-centered redox processes, and the dash-dot line shows the E$_{1/2}$ of ferrocene oxidation in both samples.

Both [3]rotaxanes **3·(Cl)$_2$** and **3·(PF$_6$)$_2$** exhibited a similar voltammographic response (Figure 5). A number of closely spaced reduction processes were observed in each case, corresponding to sequential addition of an electron on either a C$_{60}$ fullerene or NDI moiety. Square wave voltammetry was used to determine the redox potential values for closely overlapping peaks (Figures S11 and S12). Careful comparison of the observed reduction potentials with those measured in the corresponding building block compounds, as well as closely related structures reported in the literature, permitted assignment of processes at –0.81 V (–0.82), –1.25 V (–1.27 V)[64] and –1.82 V as fullerene C$_{60}^-$/C$_{60}$, C$_{60}^{2-}$/C$_{60}^-$ and C$_{60}^{3-}$/C$_{60}^{2-}$ redox couples for non-coordinating (and coordinating) anion salts respectively.[35] Similarly, peaks at –0.96 V and –1.41 V (–1.32 V) were assigned as NDI$^-$/NDI and NDI^{2-}/NDI$^-$ redox couples,[65] whilst the single oxidation process observed at +0.07 V (+0.03 V) was associated with the Fc$^+$/Fc redox couple of the ferrocenyl macrocycle components. Importantly, the oxidation of NDI, biphenyl or hydroquinone units was not observed, and the triazolium unit reduction was only observed at –2.09 V which is a significantly more cathodic potential value than the 3rd reduction potential of the fullerene cage.

The potential of each redox couple in the [3]rotaxanes was largely unperturbed in comparison to the individual methanofullerene, NDI and ferrocene building blocks such that the voltammographic response was in general a superposition of the redox processes of the individual donor/acceptor components (Table 1 and ESI). Furthermore, comparison of each redox couple in the [3]rotaxane with the corresponding axle or macrocycle component redox couple values also revealed only small cathodic or anodic shifts for the reduction or oxidation processes, respectively (Table 1). Therefore, consistent with observations from steady state absorption spectroscopy (*vide supra*), this confirms the presence of only a weak ground state electronic interaction between interlocked components within the [3]rotaxane.

As expected from ^{1}H NMR spectroscopy (*vide supra*), a 40 mV cathodic shift of the Fc$^+$/Fc redox couple from **3·(PF$_6$)$_2$** versus **3·(Cl)$_2$** was exhibited due to chloride halide binding in the conjugated ferrocenyl–isophthalamide-containing cavity of the macrocycle.[52] However, since anion recognition does not occur directly at any of the acceptor C$_{60}$ fullerene and NDI motifs, anion exchange of [3]rotaxane **3·(A)$_2$** produced only a minor difference in the redox potential position of the first and second reduction processes, confirming that anion exchange induces only a small effect on the ground state electronic structure of the system.

The potentials of each redox couple allowed the HOMO–LUMO gap and the energies of other frontier orbitals to be estimated for [3]rotaxanes **3·(Cl)$_2$** and **3·(PF$_6$)$_2$.** For both salts, the LUMO is localized on C$_{60}$

fullerene, however the first reduction processes of the C_{60} and NDI are very close in energy, and separated by only ~0.15 eV. Therefore, both [3]rotaxanes can be considered as a donor–acceptor–*stronger acceptor* system. The small HOMO (ferrocene)–LUMO gaps of 0.85 eV ($\mathbf{3 \cdot (Cl)_2}$) and 0.88 eV ($\mathbf{3 \cdot (PF_6)_2}$) indicated that excited state charge–transfer processes were energetically favorable over formation of $^3C_{60}^*$ (1.5 eV);[66] with the lowest energy charge–separated state being [$C_{60}^{\cdot-}$–Fc$^+$]. However, electron transfer to the NDI was also possible; with [NDI$^{\cdot-}$–Fc$^+$] being marginally higher in energy (0.99 eV for $\mathbf{3 \cdot (Cl)_2}$ and 1.04 eV for $\mathbf{3 \cdot (PF_6)_2}$). This suggested the possibility of competitive photoinduced electron transfer processes within the system, as well as consecutive electron transfer to form charge separated states of differing nature and composition.[40] Therefore, the effect of the co-conformational change on the photophysical behavior of the [3]rotaxane was investigated via a diverse set of time-resolved methods (*vide infra*).

Fluorescence spectroscopy

Initially, fluorescence spectroscopy was used to probe the effect of anion induced co-conformational switching on the excited state of the [3]rotaxane. Emission spectra were recorded for each salt $\mathbf{3 \cdot (Cl)_2}$ and $\mathbf{3 \cdot (PF_6)_2}$ in CHCl$_3$ (50 µM) upon excitation at 300-500 nm to study both NDI[57] and C_{60} fullerene[67] electron-deficient fluorophores in the system (Figures 6, S13 and S14). Most notably a strong emission band was observed for $\mathbf{3 \cdot (Cl)_2}$ centered at 435 nm with vibrational progression characteristic of a non-core functionalized NDI derivative (Figure 6b).[57,68,69] By stark contrast, the same NDI emission band was significantly quenched in $\mathbf{3 \cdot (PF_6)_2}$ (Figure 6b). Therefore, chloride induced co-conformational switching in the [3]rotaxane elicited a greater than three-fold enhancement in the fluorescence quantum yield that was large enough to be visible to the naked-eye (Figure 6b and SI Section 7).[70] Control fluorescence spectroscopic studies with axle components $\mathbf{1 \cdot (Cl)_2}$ and $\mathbf{1 \cdot (PF_6)_2}$ revealed a negligible anion dependence to the emission spectra (Figure S15) indicating that the controlled, reversible and large-amplitude anion-induced translational motion of the ferrocene-based macrocycle components is integral in defining the distinct 'on-off' fluorescence response of the [3]rotaxane shuttle (Figure 6a).

The efficient quenching of the NDI fluorescence emission in the co-conformer of $\mathbf{3 \cdot (PF_6)_2}$ may be explained by photoinduced electron transfer (PET) from a ferrocenyl donor group to the proximal NDI acceptor station at which the macrocycle resides. Whilst electrochemical analysis of the donor and acceptor components showed that PET was thermodynamically favorable in the [3]rotaxane, the formation of such charge-separated states has been previously reported in Fc–NDI donor–acceptor systems.[71-75] The characteristic charge–transfer-to-NDI emission is typically observed as a featureless band centered at ~550 nm,[76] and indeed such a peak was observed for $\mathbf{3 \cdot (PF_6)_2}$ upon excitation (λ_{ex} = 400-500 nm, Figure S14). By contrast, the co-conformation of bis-chloride salt $\mathbf{3 \cdot (Cl)_2}$ results in each Fc donor-containing macrocycle being spatially removed from the peripheral NDI axle stations making a long distance through-space electron transfer and quenching of the photoexcited NDI kinetically disfavored relative to PET to the nearby C_{60} fullerene acceptor.[77] Furthermore, an additional thermodynamic driving force for the latter process exists on account of C_{60} being a stronger acceptor than NDI (*vide supra*). A variety of transient spectroscopic techniques were thus employed to probe the role of C_{60} fullerene and delve further into the mechanisms behind the distinct photophysical behavior of the multicomponent [3]rotaxane shuttle in each anion state.
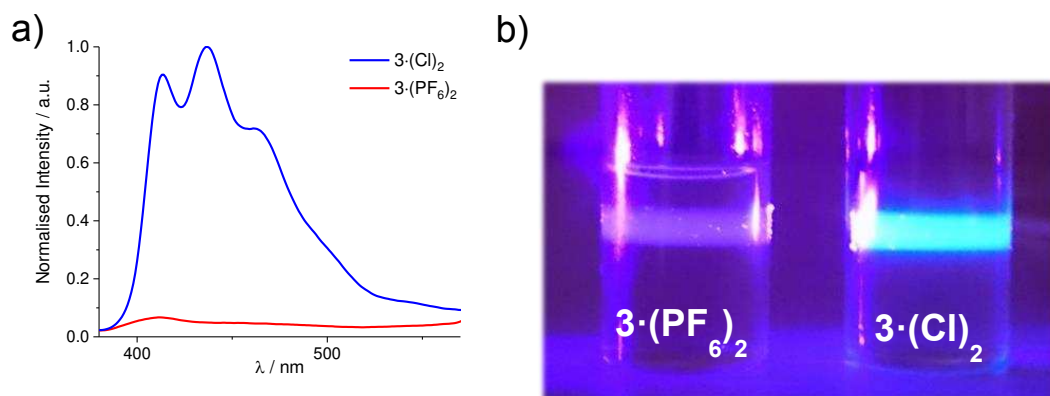
Figure 6. a) Fluorescence spectra for $\mathbf{3 \cdot (Cl)_2}$ and $\mathbf{3 \cdot (PF_6)_2}$ in CHCl$_3$, 50 µM, λ_{ex} = 300 nm showing the NDI-specific emission. b) Switching-on of fluorescent response is visible to the naked-eye in CHCl$_3$, 50 µM, λ_{ex} = 400 nm with a laser.

11

Transient absorption spectroscopy

To elucidate the photoinduced processes in these systems, transient absorption spectroscopy (TA) in visible and near-infrared (NIR) regions was used. Transient absorption spectra of $3 \cdot (Cl)_2$ and $3 \cdot (PF_6)_2$ were recorded in dichloromethane solution upon 400 nm, ~50 fs excitation at various time delays (Figures 7 and SI Section 8). Global fit analysis of the TA spectra of $3 \cdot (Cl)_2$ and $3 \cdot (PF_6)_2$ showed several components for both [3]rotaxane salts, however the contribution of each component to the overall decay was dictated by the anion dependent co-conformation. The first component in each case is ultrafast (~0.5 ps, and most likely corresponds to the formation of $^1NDI^*$ (3.22 eV) or $^1C_{60}^*$ (1.80 eV), convolved with coherent processes, and will not be discussed further).

At early time delays of a few picoseconds, the spectrum of $3 \cdot (PF_6)_2$ in the visible region is consistent with the formation of NDI^-, showing characteristic bands at 470 and 610 nm (Figure 7a, black line).[78] These features are short lived (~8 ps), and most likely correspond to the formation of $[NDI^- - Fc^+]$ charge separated state (1.04 eV). This supports the fluorescence spectroscopy observations, which indicated quenching of the NDI emission due to PET (*vide supra*). The absorption signature of the Fc^+ within the detection window is at ca. 620 nm, although is known to have a low extinction coefficient (~500 $M^{-1}cm^{-1}$)[79] and is therefore masked by a strong-absorbing NDI^- when the latter is present. However, clearly evident is the fact that the intensity of the ~620 nm band at early time delays is higher than would be expected from the NDI^- spectrum, indicating that the Fc^+ was indeed evolved.

At longer time-delays a new excited state develops with a lifetime of >400 ps[80] (Figure 7a, blue line). Comparison of the evolved spectral shape with the Decay Associated Spectra (DAS) reported for a similar covalently linked C_{60}–NDI–Fc triad suggests electron shift from NDI^- to a stronger C_{60} fullerene acceptor and concomitant formation of a new $[C_{60}^- - Fc^+]$ charge-separated state (0.88 eV).[40] Analysis of the spectral changes in the NIR region supports this assumption (Figure 7d). C_{60} fullerene radical-anion (C_{60}^-) is known to possess a characteristic NIR signature absorption, the position of which changes depending on the type of functionalization of the cage from ~1010 nm in fulleropyrrolidine[81,82] to ~1040-1050 nm in methanofullerenes[83,84] and ~1080 nm in pristine C_{60}.[85–87] In $3 \cdot (PF_6)_2$ a clear NIR absorption is detected at 1050 nm at later delay times, consistent with the radical-anion of a methanofullerene (Figure 7b, blue line), which is also present, but less pronounced at early time delays (Figure 7b, black line). This confirms the initial formation of NDI^- followed by an electron shift to C_{60} fullerene and generation of C_{60}^-. The fact the NIR absorption signature of C_{60}^- was also observed at very early time delays suggests two independent channels populating C_{60}^-. Indeed, 400 nm excitation may result in excitation of either NDI or C_{60} acceptors, yielding either $^1NDI^*$ or $^1C_{60}^*$, both of which could lead to formation of C_{60}^-.

Global fit analysis of the [3]rotaxane bis-chloride salt dynamics also reveal the presence of several components. The spectrum corresponding to the fast decay component in $3 \cdot (Cl)_2$ is different from that in $3 \cdot (PF_6)_2$ (Figure 7c, blue line). In the fast component (~5 ps) the presence of the NDI^- absorption signature is not observed, implying that the NDI is not involved in any charge transfer processes. This supports the steady-state fluorescence spectroscopy observations (*vide supra*), in which $3 \cdot (Cl)_2$ exhibited strong, structured fluorescence of NDI (Figure 6b). At later times the spectral shape evolves (Figure 7c, red line), and is nearly identical to the slow component in $3 \cdot (PF_6)_2$, implying electron transfer from the ferrocene donor to C_{60} occurs to form a $[C_{60}^- - Fc^+]$ charge-separated state (0.85 eV). Consequently the NIR region also shows evolution of the peak at 1050 nm characteristic of a methanofullerene C_{60}^- (Figure 7d, blue line) which, by contrast to $3 \cdot (PF_6)_2$, is distinct from early time delays. The transient absorption spectra of both [3]rotaxanes at late times (> 50 ps) are very similar to one another, indicating that the lowest energy excited state is the same in both cases.
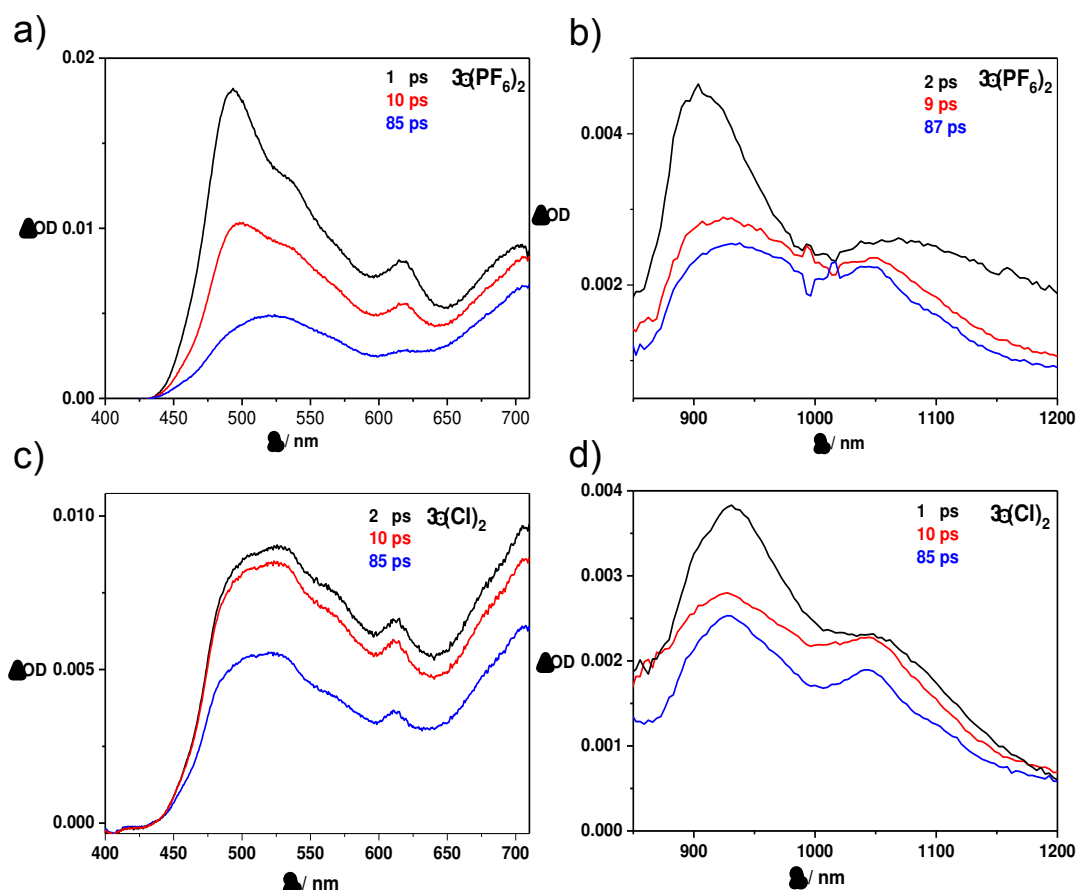
Figure 7. Electronic transient absorption spectra of solutions of **3·(PF$_6$)$_2$** (top) and **3·(Cl)$_2$** (bottom) in dichloromethane at r.t., in visible and NIR regions, recorded at indicated time delays upon excitation with ~50 fs, 400 nm laser pulse.

Time-resolved infrared spectroscopy

The photoinduced processes in the two [3]rotaxane salts were also probed by time-resolved infrared spectroscopy (TRIR) upon excitation with ~40 fs, 400 nm laser pulse in dichloromethane (Figure 8 and SI Section 9). The ground state IR spectra of all compounds are shown in the SI (Figure S10). Early time delay spectra of both **3·(PF$_6$)$_2$** and **3·(Cl)$_2$** show bleach of 1706 cm^{-1} and 1666 cm^{-1}, 1740 cm^{-1}, and 1645 cm^{-1} indicating that 400 nm excitation affects both C$_{60}$ and NDI moieties, however, the spectral shape and spectral dynamics are strongly dependent on the counterion and thus co-conformation of the system.

For **3·(PF$_6$)$_2$**, transient bands are observed at 1516, 1576 and 1623 cm^{-1}, all characteristic of the NDI radical-anion (NDI$^{\cdot-}$),[65] as well as an intense band centered at ~1500 cm^{-1} which is composed of several overlapping vibrational transitions (Figure 8a). This transient band overlaps with a 1500 cm^{-1} bleach of a vibration localized on a phenyl ring. The spectrum decays synchronously across the probed region, with the exception of a small evolution at ~1585 cm^{-1} and which may be attributed to minor changes of electron density distribution on NDI. This supports the TA and fluorescence spectroscopy data, in which charge transfer and formation of NDI$^{\cdot-}$ was observed (*vide supra*). For **3·(Cl)$_2$**, a large positive signal of the IR absorbance of C$_{60}{}^{\cdot-}$ was observed since early times, indicating the charge-transfer to fullerene and formation of a charge separated state (Figure 8b).[88]

Overall, the TRIR results unequivocally confirm electron transfer to NDI and C_{60} in case of **3(PF₆)₂** and **3(Cl)₂** respectively. This is in direct agreement with conclusions from fluorescence emission and TA spectroscopy in which the hexafluorophosphate co-conformation of the [3]rotaxane (**3(PF₆)₂**) results in formation of an excited state containing NDI⁻ and Fc·⁺ but by contrast the contribution of this channel is <5% when the anion is switched to chloride. Importantly, this is consistent with the 5% occupancy of the ferrocenyl-containing macrocycles at the NDI stations in **3(Cl)₂** obtained previously by ¹H NMR spectroscopy (Figure 4).
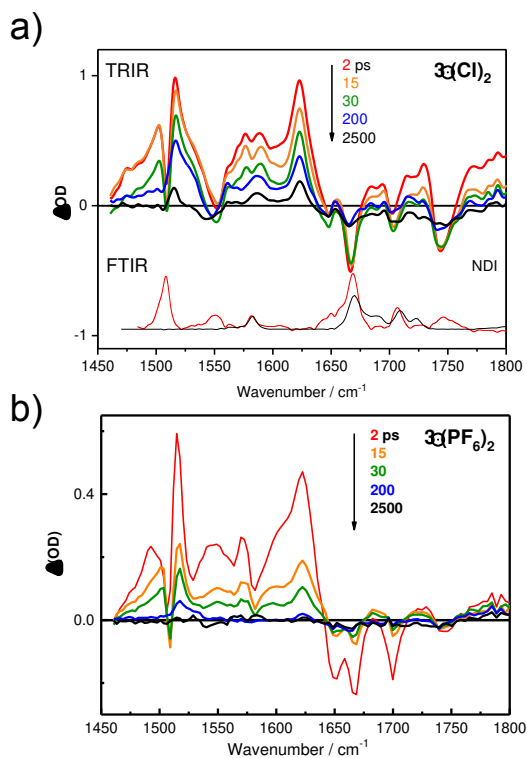

Figure 8. TRIR spectral changes in a) **3·(Cl)₂** and b) **3·(PF₆)₂** recorded in 0.1 mM dichloromethane solutions upon excitation with ~40 fs, 400 nm laser pulse at specified time delays. The bottom panel in (a) also shows an FTIR spectrum of **3·(Cl)₂** (red) and an *N,N'*-dioctyl-NDI[65,89] (black).
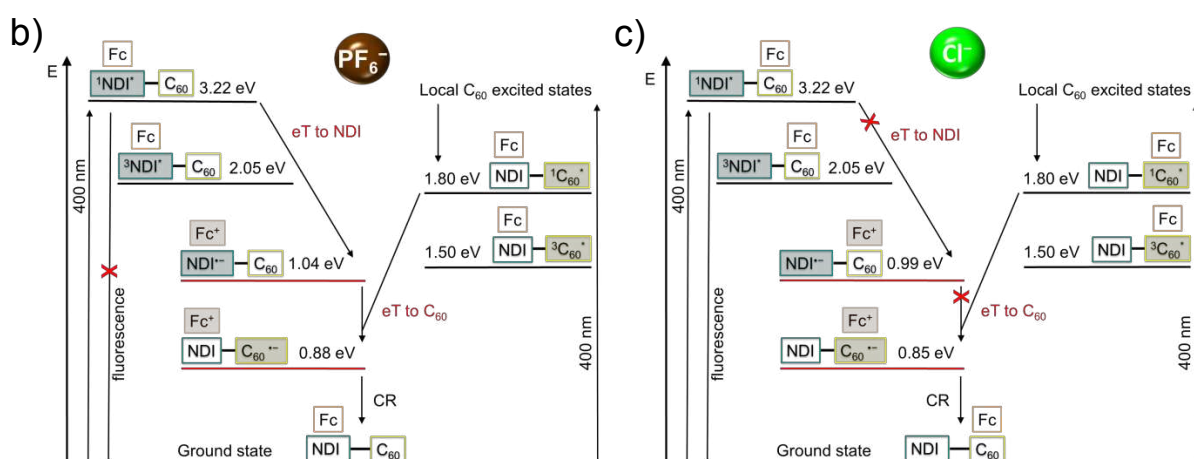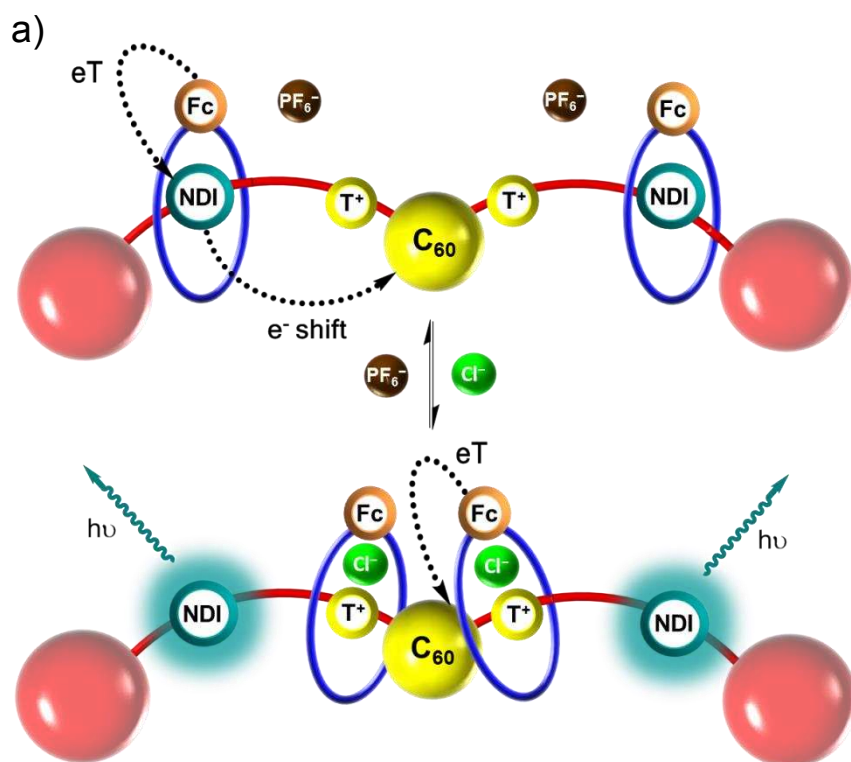
Figure 9. a) Schematic of the dynamic D–A four-station C_{60} fullerene-containing [3]rotaxane and NDI fluorescence response and electron transfer processes switchable via anion induced molecular motion. Proposed energy level diagrams of the photoinduced processes in b) $3 \cdot (PF_6)_2$ and c) $3 \cdot (Cl)_2$. NDI = naphthalene diimide, T^+ = triazolium, Fc = ferrocene, CR = charge recombination and eT = electron transfer.

Figure 9 shows the proposed energy level diagrams of the photoinduced processes in [3]rotaxanes $3 \cdot (PF_6)_2$ and $3 \cdot (Cl)_2$ highlighting the effect of large-amplitude anion mediated co-conformational change via translational motion on the photophysical response of the system. The final charge separated state, namely $[C_{60}{}^{\cdot-}–Fc^{\cdot+}]$, is the same in nature in both salts and the lifetimes differ slightly, however, the dynamics are different, and the energy redistribution pathway upon photoexcitation varies drastically. Therefore, in $3 \cdot (PF_6)_2$ both NDI and C_{60} act as electron acceptors, resulting in efficient quenching of the NDI fluorescence and initial formation of NDI$^{\cdot-}$, followed by an electron shift to C_{60} fullerene. The spatial proximity of the Fc donor and NDI acceptor thus allows formation of the higher energy charge separated state $[NDI^{\cdot-}–Fc^{\cdot+}]$. By contrast, in $3 \cdot (Cl)_2$ the NDI moiety does not participate in electron transfer, and PET results in generation of the lowest energy C_{60} fullerene-based charge separated state $[C_{60}{}^{\cdot-}–Fc^{\cdot+}]$, comparable to a 'thermodynamic' product. Critically, such contrasting photophysical behavior is mediated by anion induced co-conformational change of the multicomponent [3]rotaxane molecular shuttle via translational motion of the electron donating macrocycles between the electron accepting stations of the axle component.

15

Conclusions

In the pursuit of artificial, switchable photoactive devices[31,47,90–95] we have designed a novel, multicomponent [3]rotaxane molecular shuttle consisting of a four station bis-naphthalene diimide and C_{60} fullerene bis-triazolium axle component, and two mechanically bonded ferrocenyl-isophthalamide anion binding site-containing macrocycles, prepared via an anion template synthetic methodology. The [3]rotaxane was isolated as its coordinating (chloride) and non-coordinating (hexafluorophosphate) salts, each with a discrete interlocked co-conformation which serves to change the positions of the electron donor and acceptor motifs incorporated into the mechanically bonded macrocycle and axle components. Comprehensive one- and two-dimensional ^{1}H NMR spectroscopy was used to characterize the large-amplitude anion-mediated translational motion of the macrocycle components that interconverts these co-conformations with high positional integrity. This was critical if each co-conformational state was to exhibit distinct photophysical behavior.

As such, anion exchange of the [3]rotaxane triggered a naked-eye on/off switch of the fluorescence response which, via electrochemical analysis and absorption and emission spectroscopies, could be rationalized by distant-dependent photo-induced electron transfer from the ferrocenyl donor group of a macrocyclic ring to an NDI acceptor station of the axle component. Detailed time-resolved UV–Vis absorption and infrared spectroscopies were employed to probe each co-conformation of the [3]rotaxane shuttle and elucidate pathways by which the excited state decays in each case. These studies clearly demonstrated that the [3]rotaxane chloride co-conformation, in which the macrocycles reside at the center of the axle component, precludes electron transfer to NDI, resulting in the switching-on of emission from the NDI fluorophore and concommitant formation of a C_{60} fullerene-based charge separated state. By stark contrast, in the absence of chloride as the hexafluorophosphate salt, the macrocycles to shuttle to the peripheral NDI stations, quenching NDI emission via formation of an NDI-containing charge separated state. Importantly, in this co-conformation, the [$NDI^{\cdot-}$–$Fc^{\cdot+}$] charge separated state is accessible and initially populated, even though it is higher in energy than the alternative [$C_{60}^{\cdot-}$–$Fc^{\cdot+}$] species. Therefore, selectivity between the initially populated charge separated state in the [3]rotaxane shuttle is enabled by anion induced co-conformational switching and alteration of communication pathways operating between electron donor and acceptor motifs. To the best of our knowledge, control over the photophysical behavior of a higher-order mechanically interlocked molecular machine in this fashion is unprecedented. Such dynamic MIM systems of this design will further stimulate their exploitation both as components in artificial photosynthetic devices and as next generation photoactive anion sensors.

Associated Content

Further details of synthetic procedures, characterization, electrochemical and spectroscopic data, including Figures S1 – S20, are included in the Supporting Information.

Author Information

Corresponding Author

*paul.beer@chem.ox.ac.uk

ORCID:

Paul D. Beer: 0000-0003-0810-9716

Julia A. Weinstein: 0000-0001-6883-072X

Timothy A. Barendt: 0000-0002-9806-4381

Maria A. Lebedeva: 0000-0002-3543-6416

Ilija Rašović: 0000-0001-9466-6281

Acknowledgements

References

(1)   Sauvage, J.-P. *Angew. Chem. Int. Ed.* **2017**, 56, 11080.
(2)   Stoddart, J. F. *Angew. Chem. Int. Ed.* **2017**, 56, 11094.
(3)   Feringa, B. L. *Angew. Chem. Int. Ed.* **2017**, 56, 11060.
(4)   Stoddart, J. F. *Acc. Chem. Res.* **2001**, 34, 410.
(5)   Kay, E. R.; Leigh, D. A. *Angew. Chem. Int. Ed.* **2015**, 54, 10080.
(6)   Bruns, C. J.; Stoddart, J. F. In *The Nature of the Mechanical Bond*; John Wiley & Sons, Inc., Hoboken, NJ, **2016**.
(7)   Neal, E. A.; Goldup, S. M. *Chem. Commun.* **2014**, 50, 5128.
(8)   Erbas-Cakmak, S.; Leigh, D. A.; McTernan, C. T.; Nussbaumer, A. L. *Chem. Rev.* **2015**, 115, 10081.
(9)   Kay, E. R.; Leigh, D. A.; Zerbetto, F. *Angew. Chem. Int. Ed.* **2007**, 46, 72.
(10)   Stoddart, J. F. *Chem. Soc. Rev.* **2009**, 38, 1802.
(11)   Saha, S.; Stoddart, J. F. *Chem. Soc. Rev.* **2006**, 36, 77.
(12)   Balzani, V.; Clemente-León, M.; Credi, A.; Ferrer, B.; Venturi, M.; Flood, A. H.; Stoddart, J. F. *Proc. Natl. Acad. Sci.* **2006**, 103, 1178.
(13)   Wang, Q.-C.; Qu, D.-H.; Ren, J.; Chen, K.; Tian, H. *Angew. Chem. Int. Ed.* **2004**, 43, 2661.
(14)   Raiteri, P.; Bussi, G.; Cucinotta, C. S.; Credi, A.; Stoddart, J. F.; Parrinello, M. *Angew. Chem. Int. Ed.* **2008**, 47, 3536.
(15)   Brouwer, A. M.; Frochot, C.; Gatti, F. G.; Leigh, D. A.; Mottier, L.; Paolucci, F.; Roffia, S.; Wurpel, G. W. H. *Science* **2001**, 291, 2124.
(16)   Marlin, D. S.; González Cabrera, D.; Leigh, D. A.; Slawin, A. M. Z. *Angew. Chem. Int. Ed.* **2006**, 45, 77.
(17)   Berná, J.; Alajarín, M.; Orenes, R.-A. *J. Am. Chem. Soc.* **2010**, 132, 10741.
(18)   Barendt, T. A.; Robinson, S. W.; Beer, P. D. *Chem. Sci.* **2016**, 7, 5171.
(19)   Liu, L.; Liu, Y.; Liu, P.; Wu, J.; Guan, Y.; Hu, X.; Lin, C.; Yang, Y.; Sun, X.; Ma, J.; Wang, L. *Chem. Sci.* **2013**, 4, 1701.
(20)   Spence, G. T.; Pitak, M. B.; Beer, P. D. *Chem. – Eur. J.* **2012**, 18, 7100.
(21)   Evans, N. H.; Serpell, C. J.; Beer, P. D. *Chem. – Eur. J.* **2011**, 17, 7734.
(22)   Gassensmith, J. J.; Matthys, S.; Lee, J.-J.; Wojcik, A.; Kamat, P. V.; Smith, B. D. *Chem. – Eur. J.* **2010**, 16, 2916.
(23)   Lin, T.-C.; Lai, C.-C.; Chiu, S.-H. *Org. Lett.* **2009**, 11, 613.
(24)   Barrell, M. J.; Leigh, D. A.; Lusby, P. J.; Slawin, A. M. Z. *Angew. Chem. Int. Ed.* **2008**, 47, 8036.
(25)   Lin, C.-F.; Lai, C.-C.; Liu, Y.-H.; Peng, S.-M.; Chiu, S.-H. *Chem. – Eur. J.* **2007**, 13, 4350.
(26)   Huang, Y.-L.; Hung, W.-C.; Lai, C.-C.; Liu, Y.-H.; Peng, S.-M.; Chiu, S.-H. *Angew. Chem. Int. Ed.* **2007**, 46, 6629.
(27)   Andrievsky, A.; Ahuis, F.; Sessler, J. L.; Vögtle, F.; Gudat, D.; Moini, M. *J. Am. Chem. Soc.* **1998**, 120, 9712.
(28)   For examples of non-interlocked anion switches see: (a) Zhao, W.; Qiao, B.; Chen, C.-H.; Flood, A. H. *Angew. Chem. Int. Ed.* **2017**, 56, 13083. (b) Suk, J.; Naidu, V. R.; Liu, X.; Lah, M. S.; Jeong, K.-S. *J. Am. Chem. Soc.* **2011**, 133, 13938. (c) Gavette, J. V.; Mills, N. S.; Zakharov, L. N.; Johnson, C. A.; Johnson, D. W.; Haley, M. M. *Angew. Chem. Int. Ed.* **2013**, 52, 10270. (d) Wezenberg, S. J.; Feringa, B. L. *Org. Lett.* **2017**, 19, 324.
(29)   Barendt, T. A.; Docker, A.; Marques, I.; Félix, V.; Beer, P. D. *Angew. Chem. Int. Ed.* **2016**, 55, 11069.
(30)   Barendt, T. A.; Ferreira, L.; Marques, I.; Félix, V.; Beer, P. D. *J. Am. Chem. Soc.* **2017**, 139, 9026.
(31)   Balzani, V.; Credi, A.; Venturi, M. *Chem. Soc. Rev.* **2009**, 38, 1542.
(32)   Kroto, H. W.; Heath, J. R.; O'Brien, S. C.; Curl, R. F.; Smalley, R. E. *Nature* **1985**, 318, 162.
(33)   Mateo-alonso, A. In *Supramolecular Chemistry of Fullerenes and Carbon Nanotubes*; Nazariortín, Nierengarten, J.-F., Eds.; Wiley-VCH Verlag GmbH & Co. KGaA, Weinheim, Germany, **2012**; pp 107–126.
(34)   Mateo-Alonso, A. *Chem. Commun.* **2010**, 46, 9089.
(35)   Echegoyen, L.; Echegoyen, L. E. *Acc. Chem. Res.* **1998**, 31, 593.
(36)   Xie, Q.; Perez-Cordero, E.; Echegoyen, L. *J. Am. Chem. Soc.* **1992**, 114, 3978.
(37)   Dubois, D.; Kadish, K. M.; Flanagan, S.; Haufler, R. E.; Chibante, L. P. F.; Wilson, L. J. *J. Am. Chem. Soc.* **1991**, 113, 4364.
(38)   Dubois, D.; Kadish, K. M.; Flanagan, S.; Wilson, L. J. *J. Am. Chem. Soc.* **1991**, 113, 7773.

(39)   Lebedeva, M. A.; Chamberlain, T. W.; Khlobystov, A. N. *Chem. Rev.* **2015**, 115, 11301.

(40)   Supur, M.; El-Khouly, M. E.; Seok, J. H.; Kay, K. Y.; Fukuzumi, S. *J. Phys. Chem. A* **2011**, 115, 14430.

(41)   Zandler, M. E.; Smith, P. M.; Fujitsuka, M.; Ito, O.; D'Souza, F. *J. Org. Chem.* **2002**, 67, 9122.

(42)   D'Souza, F.; Ito, O. *Chem. Commun.* **2009**, 4913.

(43)   Martín, N.; Sánchez, L.; Herranz, M. Á.; Illescas, B.; Guldi, D. M. *Acc. Chem. Res.* **2007**, 40, 1015.

(44)   Karlsson, S.; Modin, J.; Becker, H.-C.; Hammarström, L.; Grennberg, H. *Inorg. Chem.* **2008**, 47, 7286.

(45)   Kirner, S. V.; Henkel, C.; Guldi, D. M.; Megiatto Jr, J. D.; Schuster, D. I. *Chem Sci* **2015**, 6, 7293.

(46)   Diederich, F.; Dietrich-Buchecker, C.; Nierengarten, J.-F.; Sauvage, J.-P. *J. Chem. Soc. Chem. Commun.* **1995**, 7, 781.

(47)   Megiatto, J. Jackson D.; Schuster, D. I. In *RSC Nanoscience & Nanotechnology*; Langa De La Puente, F., Nierengarten, J.-F., Eds.; Royal Society of Chemistry: Cambridge, **2011**; pp 354–385.

(48)   *The Photosynthetic reaction center*; Deisenhofer, J., Norris, J. R., Eds.; Academic Press: San Diego, CA, **1993**.

(49)   Mateo-Alonso, A.; Ehli, C.; Rahman, G. M. A.; Guldi, D. M.; Fioravanti, G.; Marcaccio, M.; Paolucci, F.; Prato, M. *Angew. Chem. Int. Ed.* **2007**, 46, 3521.

(50)   Pereira de Freitas, R.; Iehl, J.; Delavaux-Nicot, B.; Nierengarten, J.-F. *Tetrahedron* **2008**, 64, 11409.

(51)   Bingel, C. *Chem. Ber.* **1993**, 126, 1957.

(52)   Evans, N. H.; Beer, P. D. *Org. Biomol. Chem.* **2010**, 9, 92.

(53)   Gomes, J. A. N. F.; Mallion, R. B. *Chem. Rev.* **2001**, 101, 1349.

(54)   Prato, M.; Suzuki, T.; Wudl, F.; Lucchini, V.; Maggini, M. *J. Am. Chem. Soc.* **1993**, 115, 7876.

(55)   This upfield shift is 0.15 ppm larger than in a related [2]rotaxane that does not contain a C_{60} fullerene.[18]

(56)   Baggerman, J.; Jagesar, D. C.; Vallée, R. A. L.; Hofkens, J.; De Schryver, F. C.; Schelhase, F.; Vögtle, F.; Brouwer, A. M. *Chem. – Eur. J.* **2007**, 13, 1291.

(57)   Bhosale, S. V.; Jani, C. H.; Langford, S. J. *Chem. Soc. Rev.* **2008**, 37, 331.

(58)   Snow, S. D.; Lee, J.; Kim, J.-H. *Environ. Sci. Technol.* **2012**, 46, 13227.

(59)   Leach, S.; Vervloet, M.; Desprès, A.; Bréheret, E.; Hare, J. P.; John Dennis, T.; Kroto, H. W.; Taylor, R.; Walton, D. R. M. *Chem. Phys.* **1992**, 160, 451.

(60)   Kaiser, G.; Jarrosson, T.; Otto, S.; Ng, Y.-F.; Bond, A. D.; Sanders, J. K. M. *Angew. Chem. Int. Ed.* **2004**, 43, 1959.

(61)   Dichloromethane was used instead of chloroform to avoid potential acidity and radical formation in steady state and time-resolved experiments.

(62)   Dimethylformamide was used for all electrochemical experiments to solubilize the electrolyte salts and provide a larger electrochemical potential window relative to chlorinated solvents. Established anion dependent [3]rotaxane co-conformations were maintained in this medium due to a 400-fold excess of coordinating chloride or non-coordinating tetrafluoroborate[63] anions from the supporting electrolytes compared to the [3]rotaxane salt.

(63)   Vega, I. E. D.; Gale, P. A.; Light, M. E.; Loeb, S. J. *Chem. Commun.* **2005**, 4913.

(64)   For **3·(Cl)₂** the second reduction process of C_{60} closely overlaps with the second reduction of NDI and, since it is a one-electron process, it is masked by the more pronounced two-electron NDI-based reduction. Therefore, $E_{1/2}red_2$ (C_{60}) = -1.27±0.05 V, which corresponds to half of the peak-to-peak separation of the overlapping NDI reduction.

(65)   Sazanovich, I. V.; Alamiry, M. A. H.; Best, J.; Bennett, R. D.; Bouganov, O. V.; Davies, E. S.; Grivin, V. P.; Meijer, A. J. H. M.; Plyusnin, V. F.; Ronayne, K. L.; Shelton, A. H.; Tikhomirov, S. A.; Towrie, M.; Weinstein, J. A. *Inorg. Chem.* **2008**, 47, 10432.

(66)   Hung, R. R.; Grabowski, J. J. *J. Phys. Chem.* **1991**, 95, 6073.

(67)   Catalan, J.; Elguero, J. *J. Am. Chem. Soc.* **1993**, 115, 9249.

(68)   Strong emission is relatively rare in NDI derivatives, however not unprecedented.[69]

(69)   Pandeeswar, M.; Govindaraju, T. *RSC Adv.* **2013**, 3, 11459.

(70)   Analogous to anion exchange, the addition of two equivalents of tetrabutyl ammonium chloride to **3·(PF₆)₂** elicited the same switch-on fluorescence response from the [3]rotaxane.

(71)   Takai, A.; Sakamaki, D.; Seki, S.; Matsushita, Y.; Takeuchi, M. *Chem. – Eur. J.* **2016**, 22, 7385.

(72)   Natali, M.; Ravaglia, M.; Scandola, F.; Boixel, J.; Pellegrin, Y.; Blart, E.; Odobel, F. *J. Phys. Chem. C* **2013**, 117, 19334.

(73)   Coupled with the ground state absorption and electrochemical analysis (vide supra), the broader NDI emission band of **3·(PF₆)₂** relative to **3·(Cl)₂** suggests intramolecular aromatic stacking interactions with the macrocycle may also contribute to NDI emission quenching in this co-conformation.[74,75]

(74)   Weber, G. *Trans. Faraday Soc.* **1948**, 44, 185.

(75)   Licchelli, M.; Orbelli Biroli, A.; Poggi, A. *Org. Lett.* **2006**, 8, 915.

(76) Ganesan, P.; Baggerman, J.; Zhang, H.; Sudhölter, E. J. R.; Zuilhof, H. *J. Phys. Chem. A* **2007**, 111, 6151.

(77) *Principles of Fluorescence Spectroscopy*; Lakowicz, J. R., Ed.; Springer US: Boston, MA, **2006**.

(78) Green, S.; Fox, M. A. *J. Phys. Chem.* **1995**, 99, 14752.

(79) Gray, H. B.; Sohn, Y. S.; Hendrickson, N. *J. Am. Chem. Soc.* **1971**, 93, 3603.

(80) We note that time delays longer than 200 ps have not been investigated with the TA spectroscopy and therefore values of longer lifetimes should be taken as an indication.

(81) Imahori, H.; Tamaki, K.; Guldi, D. M.; Luo, C.; Fujitsuka, M.; Ito, O.; Sakata, Y.; Fukuzumi, S. *J. Am. Chem. Soc.* **2001**, 123, 2607.

(82) Imahori, H.; Yamada, H.; Guldi, D. M.; Endo, Y.; Shimomura, A.; Kundu, S.; Yamada, K.; Okada, T.; Sakata, Y.; Fukuzumi, S. *Angew. Chem. Int. Ed.* **2002**, 41, 2344.

(83) Guldi, D. M.; Prato, M. *Acc. Chem. Res.* **2000**, 33, 695.

(84) Guldi, D. M.; Hungerbuehler, H.; Asmus, K.-D. *J. Phys. Chem.* **1995**, 99, 9380.

(85) Brezova, V.; Stasko, A.; Rapta, P.; Domschke, G.; Bartl, A.; Dunsch, L. *J. Phys. Chem.* **1995**, 99, 16234.

(86) Guldi, D. M.; Huie, R. E.; Neta, P.; Hungerbühler, H.; Asmus, K.-D. *Chem. Phys. Lett.* **1994**, 223, 511.

(87) Gasyna, Z.; Andrews, L.; Schatz, P. N. *J. Phys. Chem.* **1992**, 96, 1525.

(88) Some NDI$^{\bullet-}$-like transient bands were also observed, which we attribute to the small (5%) occupancy of the NDI station in **3·(Cl)$_2$** as determined by earlier ^{1}H NMR spectroscopic experiments (vide supra).

(89) Greenfield, S. R.; Svec, W. A.; Gosztola, D.; Wasielewski, M. R. *J. Am. Chem. Soc.* **1996**, 118, 6767.

(90) Wang, J.-Y.; Han, J.-M.; Yan, J.; Ma, Y.; Pei, J. *Chem. – Eur. J.* **2009**, 15, 3585.

(91) Ma, X.; Tian, H. *Chem. Soc. Rev.* **2009**, 39, 70.

(92) Schuster, D. I.; Li, K.; Guldi, D. M. *Comptes Rendus Chim.* **2006**, 9, 892.

(93) Guldi, D. M. *Chem. Soc. Rev.* **2002**, 31, 22.

(94) Schuster, D. I.; Cheng, P.; Jarowski, P. D.; Guldi, D. M.; Luo, C.; Echegoyen, L.; Pyo, S.; Holzwarth, A. R.; Braslavsky, S. E.; Williams, R. M.; Klihm, G. *J. Am. Chem. Soc.* **2004**, 126, 7257.

(95) Kadish, K. M.; Ruoff, R. S. *Fullerenes: Chemistry, Physics, and Technology*; John Wiley & Sons, New York, **2000**.